Density impact on toroidal rotation in Tore Supra: experimental observations and theoretical investigation

To cite this article: J Bernardo *et al* 2015 *Plasma Phys. Control. Fusion* **57** 035002

IOP Publishing Plasma Physics and Controlled Fusion

Plasma Phys. Control. Fusion **57** (2015) 035002 (11pp) doi:10.1088/0741-3335/57/3/035002

Density impact on toroidal rotation in Tore Supra: experimental observations and theoretical investigation

J Bernardo[1], C Fenzi[2], C Bourdelle[2], Y Camenen[3], H Arnichand[2], João P S Bizarro[1], S Cortes[1], X Garbet[2], Z O Guimarães-Filho[4], T Aniel[2], J-F Artaud[2], F Clairet[2], P Cottier[2], J Gunn[2], P Lotte[2] and the Tore Supra Team

[1] Instituto de Plasmas e Fusão Nuclear, Instituto Superior Técnico, Universidade de Lisboa, 1049-001 Lisboa, Portugal
[2] CEA, IRFM, F-13108 St Paul-lez-Durance, France
[3] Aix-Marseille Université, CNRS, PIIM UMR 7345, 13397 Marseille, France
[4] Instituto de Física, Universidade de São Paulo, 05315-970 São Paulo-SP, Brasil

E-mail: jbernardo@ipfn.ist.utl.pt

Received 23 July 2014, revised 31 October 2014
Accepted for publication 8 December 2014
Published 4 February 2015

Abstract

The effect of plasma density on toroidal rotation was examined in density ramp-up experiments at a plasma current of 1 MA and a toroidal magnetic field of 3.6 T in Tore Supra ohmic discharges. Experimental measurements have shown that the toroidal rotation amplitude is reduced at all radii when increasing the plasma density, although it remains in the counter-current direction. Neoclassical predictions including ripple-induced toroidal friction are in qualitative agreement with such observations. However, in the core ($r/a < 0.5$) the plasma accelerates at $n_l \sim 3 \times 10^{19}$ m^{-2} and breaks again above $n_l \sim 3.5 \times 10^{19}$ m^{-2}. This rotation bifurcation did not appear to be correlated to a possible influence of the sawtooth activity. Nonetheless, quasi-linear gyrokinetic simulations have shown that the transition of the nature of linear microinstabilities from ITG-TEM to pure ITG occurs at $n_l \sim 3 \times 10^{19}$ m^{-2}, which could indicate a change on the turbulence driven contributions and explain the deviation from neoclassical predictions in the plasma core.

Keywords: Tore Supra, intrinsic rotation, rotation bifurcation, gyrokinetic calculations

(Some figures may appear in colour only in the online journal)

1. Introduction

Velocity shear has been pointed out as a key parameter for turbulence suppression, as well as to avoid MHD instabilities such as RWMs [1] or change NTMs onset threshold [2], improving therefore the overall plasma performance. Although rotation is usually externally provided, in ITER the external torque delivered by the Neutral Beam Injection (NBI) will be rather low. Since the NBI driven rotation in ITER will be smaller than in present day devices, it is therefore of crucial importance to understand the underlying mechanisms of the so-called 'intrinsic' rotation. Intrinsic plasma rotation can be understood as resulting from the competition of various mechanisms, as turbulence [3], fast particles [4–7], MHD [8, 9] and 3D (ripple [10], RMPs [11], …) driven effects.

Rotation reversal has been reported in several machines, the direction of this reversal depends on the tokamak configuration. From co- to counter-rotation direction (with respect to the plasma current) on diverted plasmas, such as in ASDEX-Upgrade [12], C-mod [13] or TCV [14]. However, in limited plasmas, the inversion is reported to occur from counter- to co-rotation TCV [15]. The explanation for this abrupt switch on core toroidal rotation is not fully understood but has been linked to changes in density, plasma current, magnetic field and plasma shape. Specifically, rotation reversal would occur at the transition from linear ohmic confinement (LOC) to saturated

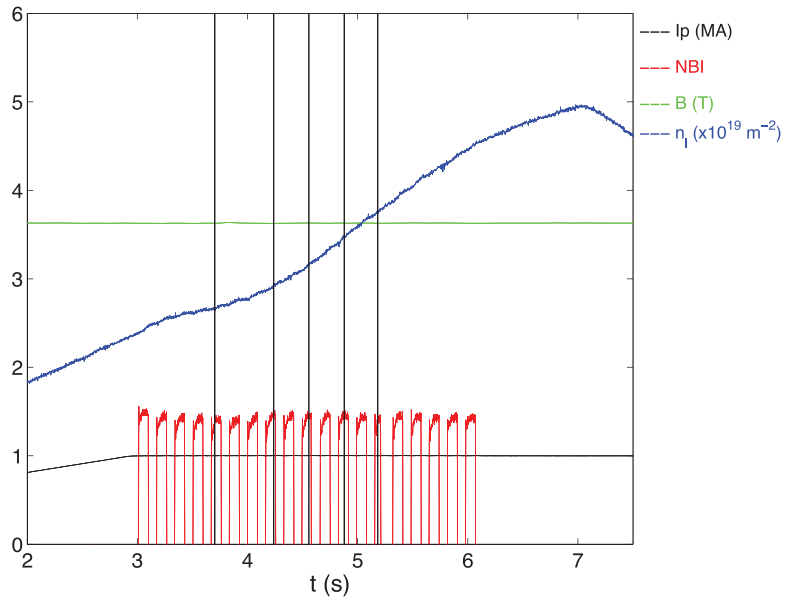

Figure 1. Time trace of plasma current (black), magnetic field (green), line integrated density (blue) and NBI blip signal (red) for Tore Supra discharge #48102.

ohmic confinement (SOC) regime [16] and the change in turbulence could be the key factor. In ASDEX-Upgrade, the turbulence regime has been clearly linked with this reversal occurrence when close to the transition between trapped electron mode (TEM) and Ion Temperature Gradient (ITG) [12]. Nonetheless, recent studies [17] indicate that changes in momentum transport do not correlate with changes in linear mode dominance. This paper is intended to clarify observations on Tore Supra rotation Ohmic L-mode discharges.

To further clarify the above mentioned subjects, plasma rotation analysis has been performed for Tore Supra limited ohmic plasmas. Tore Supra is equiped with 18 Toroidal Field (TF) coils. A finite number of TF coils induce a toroidal variation in the magnetic field, where the TF ripple amplitude is defined as $\delta_r = (B_{\max} - B_{\min})/(B_{\max} + B_{\min})$, leading in Tore Supra to values of TF ripple up to 7% at the plasma boundary. Such a high ripple makes ripple-induced toroidal friction dominant over turbulent transport processes [18].

The physical mechanisms behind the rotation bifurcation will be investigated, mainly the possible influence of sawtooth activity [19], a comparison with neoclassical predictions [20] and the role of turbulence [12, 13] on such observations. This paper is organized as follows. In section 2, a brief description is given of the plasma parameters as well as of the experimental conditions. Section 3 presents the experimental results, with the analysis of three different radial zones and evidences of core plasma toroidal rotation bifurcation in section 3.1; turbulence measurements and the analysis of normalized logarithmic gradient of different quantities focused on the core region where two rotation bifurcation are found is described in section 3.2; and the possible relationship between sawtooth activity and rotation is discussed in section 3.3. In section 4, the comparison of experimental measurements against neoclassical predictions, including ripple effects, is performed in section 4.1 and turbulence mode analysis using quasi-linear gyrokynetic simulations is explored in section 4.2, where one of the reversal is found to be linked to the transition from ITG-TEM to pure ITG. Finally, the conclusions are summarized in section 5.

2. Plasma parameters and experimental conditions

These experiments have been carried out on Tore Supra, using a set of seven limited ohmic discharges, where the plasma current I_p was 1 MA and the toroidal magnetic field 3.6 T ($q_{95} \sim 4$), both directed clockwise when viewed from top. The line integrated electron density n_l, has been assessed by the far infrared interferometer. It was varied from $n_l \sim 2.25$ to 4.9×10^{19} m^{-2} by means of deuterium gas puffing. The analyzed pulses have a circular poloidal cross-section with a major radius $R_0 = 2.37$ m and a minor radius $a = 0.7$ m, setting the TF ripple at the plasma boundary to 5% . Plasma toroidal rotation is provided by Charge eXchange Recombination Spectroscopy (CXRS) diagnostic using the CVI ($\lambda = 5290.5$ Å, $n = 8 \rightarrow 7$) spectral line analysis. The Tore Supra CXRS system has 15 tangential viewing lines with spatial resolution ranging from 2 to 6 cm [21], from the plasma edge to the core. The CXRS system uses a dedicated Diagnostic Neutral Beam injection (DNB) [22], with nearly perpendicular injection, an injected energy of 55 keV and a power of 350 kW. Since the momentum carried by the injected neutrals is rather low, it is neglected in the analysis. In these conditions the diagnostic is able to provide measurements for spontaneous toroidal rotation.

Figure 1 shows the time traces of plasma current, magnetic field, density and NBI blip signal for the Tore Supra discharge #48102, which covers the entire density range used for the analysis. In order to cover the density ramp-up, 19 NBI blips of 90 ms were performed. The sample rate of the CXRS diagnostic was set in this discharge to 66 Hz, which allows a measurement every 15 ms of the ion temperature T_i and of the

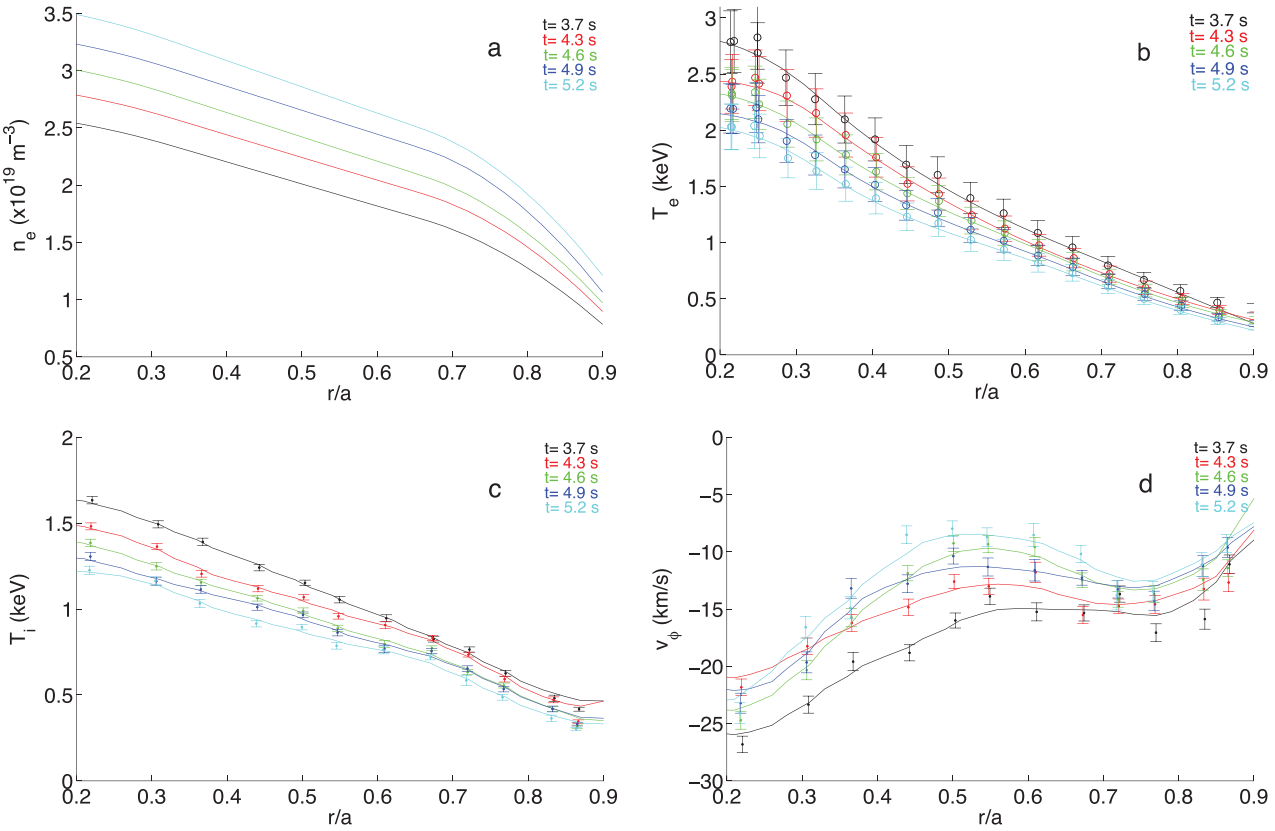

Figure 2. (*a*) Electron density, (*b*) electron temperature, (*c*) ion temperature and (*d*) toroidal velocity profiles for five time slices represented by vertical black lines in figure 1. Solid lines are intended to give a better understanding of the data point trend.

toroidal velocity (v_ϕ) of the plasma impurity ion, making possible to have about 4 profiles during each NBI blip.

To ascertain the evolution of the plasma parameters, the electron density n_e, electron temperature T_e, ion temperature T_i and toroidal velocity v_ϕ profiles are depicted in figure 2 for five time slices indicated by the vertical lines in figure 1. Electron density and temperature profiles are provided by Interferometry and Reflectometry.

The electron density profile time evolution is shown in figure 2(*a*), discussion of the evolution of the inverse gradient scale length can be found in section 3.2. On the other hand, the time evolution of temperatures (figures 2(*b*) and (*c*)) shows a decreasing temperature with increasing density. This decreasing electron temperature is more visible at the plasma core than at the edge. Regarding the toroidal velocity (figure 2(*d*)), the profiles present negative values which correspond to counter—direction with respect to the plasma current. The time evolution of these profiles indicates that as the density increases the toroidal rotation response differs from core to edge.

3. Experimental results

3.1. Plasma toroidal rotation modification with density

It is widely known that for ohmic heated discharges, at low density, the energy confinement time is proportional to the plasma density. During this LOC regime, the energy confinement time can be expressed by the Neo-Alcator scaling law [23]. Moreover, above a density threshold the energy confinement time saturates and has a weak dependence on density. In this SOC regime, the energy confinement time scales with the ITER89P scaling [24]. Experimental evidence for this transition between LOC and SOC regimes is provided in figure 3, for discharges covering the entire density ramp (#48101, #48102) with saturation density around 1.7×10^{19} m^{-3}, which corresponds to an integrated line density of 3×10^{19} m^{-2}. Furthermore, for the low density branch Tore Supra discharges, the energy confinement time presents values slightly lower than the ones predicted by the Neo-Alcator scaling law.

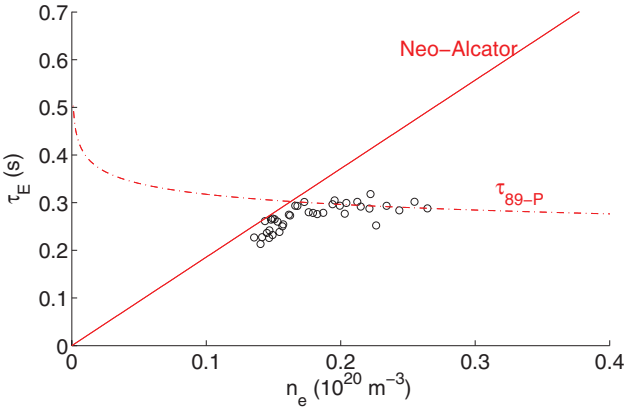

Figure 3. The energy confinement time as a function of volume averaged electron density. The solid line is the Neo-Alcator scaling law while the dashed line corresponds to the ITER89P scaling.

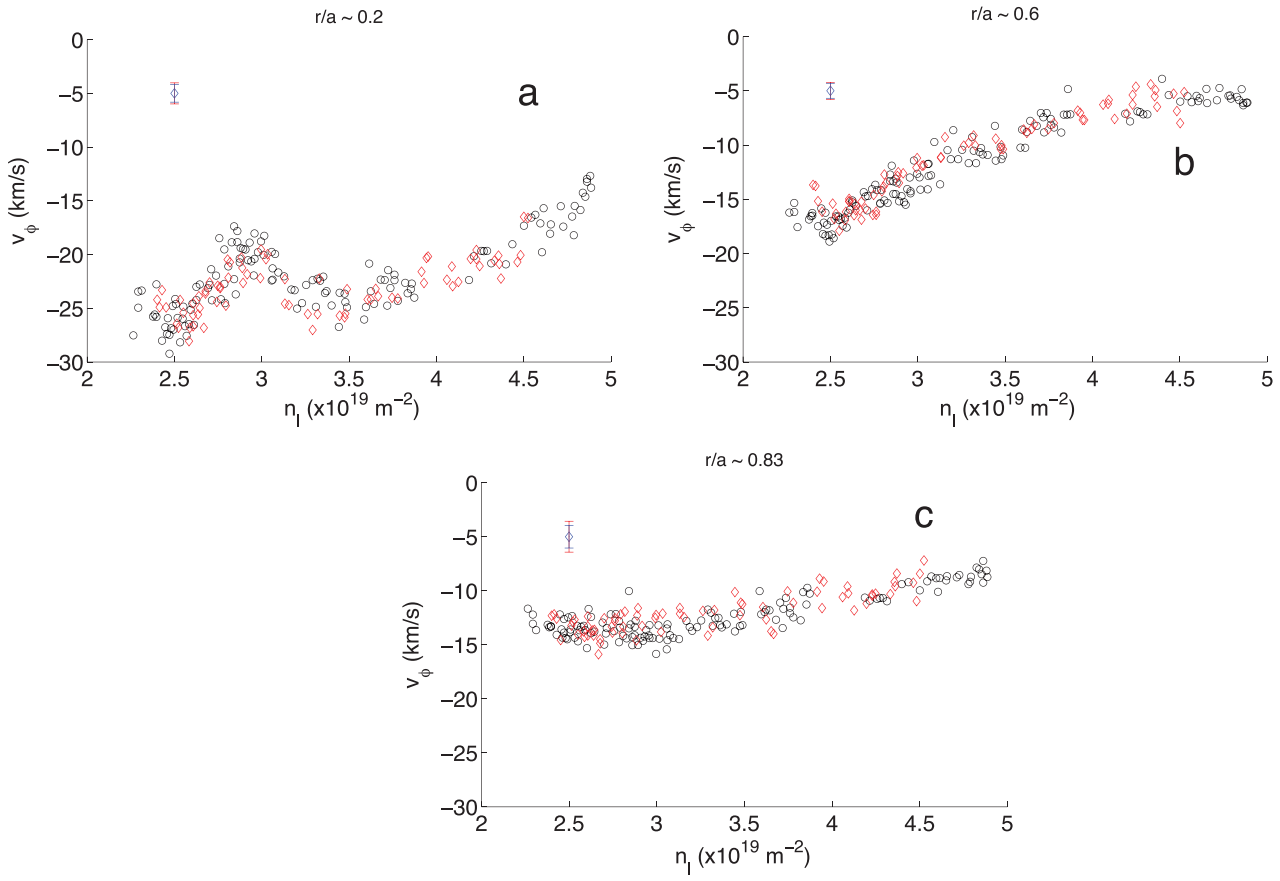

Figure 4. (*a*) Toroidal velocity at $r/a \sim 0.2$, (*b*) $r/a \sim 0.6$ and (*c*) $r/a \sim 0.83$ as a function of line integrated density for a set of 7 discharges. Red diamond symbols correspond to data from a single discharge. The blue error bar corresponds to the average errors while the red is the standard deviation.

In order to clarify the behaviour of the plasma toroidal rotation, from the plasma core to the plasma edge, during the density ramp-up, combined data from a set of six Ohmic discharges during stationary experiments have been analysed (black circles in figure 4), alongside with rotation data from a single density scan discharge covering the whole density range (red diamonds in figure 4), as a function of the integrated line density. These measurements are plotted in figure 4 for three different normalized radii plasma locations (r/a = 0.2, 0.6, 0.83), each one being representative of three distinct regions: a core region ($r/a < 0.5$, figure 4(*a*)), an intermediate region (r/a = 0.5–0.7, figure 4(*b*)) and an edge region ($r/a > 0.7$, figure 4(*c*)). From these results we can observe that rotation in the plasma core (figure 4(*a*)) changes its trend twice above specific density thresholds. First, the rotation amplitude decreases until the density reaches $n_l \sim 3 \times 10^{19}$ m^{-2}, then increases until $n_l \sim 3.5 \times 10^{19}$ m^{-2}, and decreases again for the remaining density range. This latter behaviour in the plasma core is neither observed in the intermediate (figure 4(*b*)) nor in the edge region (figure 4(*c*)). The rotation amplitude in the intermediate region seems to decrease linearly, while the density is increasing, this dependency being weaker at the edge. Note that the same rotation profiles as a function of plasma density are obtained in stationary and density ramp-up discharges demonstrating that the ramp-up phases can be considered as quasi-stationary with respect to transport.

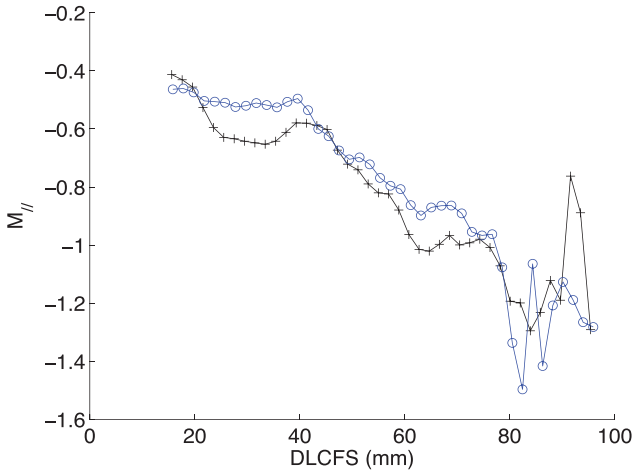

Figure 5. Parallel Mach number plotted as a function of the radial 'Distance from the LCFS' (DLCFS) at the beginning (black) and end (blue) of the density ramp-up.

Rotation observations from Tore Supra edge region have been previously reported [25], where the toroidal rotation behaviour is influenced by parallel SOL flows, which should remain unchanged during the ramp-up confirming the fact that edge toroidal rotation is constant through the discharge. Furthermore, the result depicted in figure 4(*c*) for the edge region, might be supported by the reciprocating Mach probe [26] measurements

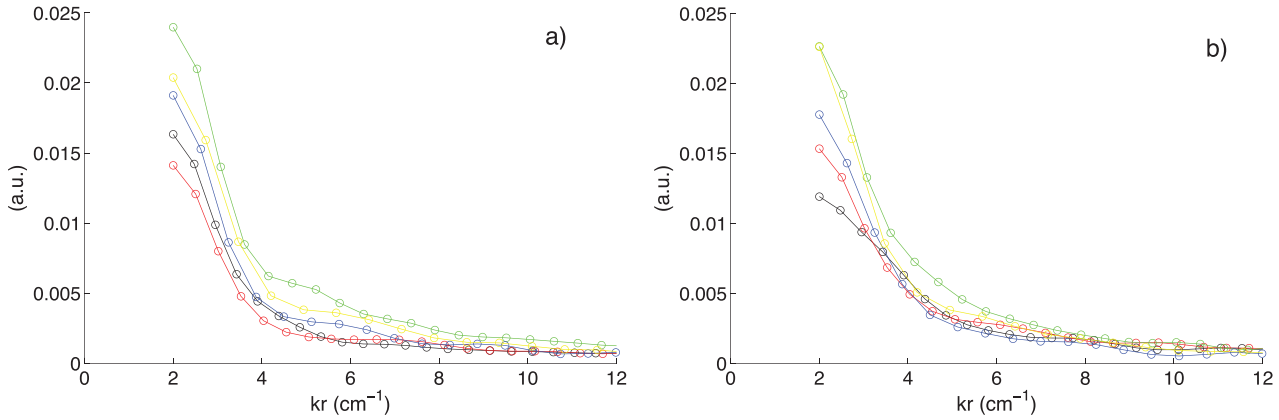

Figure 6. Wave number spectrum at $r/a = 0.67$ (*a*) and $r/a = 0.70$ (*b*) corresponding to $n_l \sim 2.38$(—), 2.69 (—), 3.11 (—), 3.82 (—) and 4.47×10^{19} mm^{-2} (—).

(see figure 5), showing no significant differences in the parallel Mach number at the beginning ($n_l \sim 2.76 \times 10^{19}$ m^{-2}) and the end ($n_l \sim 4.25 \times 10^{19}$ m^{-2}) of the density ramp-up. The measurements in the SOL region (figure 5) show essentially no distinction in behaviour between low and high density, very much like the CXRS measurements in the edge region depicted in figure 4(*c*)).

3.2. Turbulence measurements, density and temperature gradients

Tore Supra is equipped with two ultra fast-sweep reflectometers [27]. The reflected signals performed in a burst mode during unchanged plasma conditions, with a sweep time of 2 μs and a dead time between sweeps of 1 μs, allow radial profiles of the density fluctuations to be retrieved from the radial wavenumber spectra of the phase fluctuation signals [28]. Due to the plasma conditions used for this set of discharges, the experimental data only covers the plasma edge ($r/a \sim 0.64$–1). The wavenumber kr-spectra of density fluctuations (at $r/a = 0.67$ and 0.70) are depicted in figure 6, for line integrated densities of $n_l \sim 2.38$, 2.69, 3.11, 3.82 and 4.47×10^{19} m^{-2}. As one could expect, no effect is appreciable since changes in toroidal rotation are visible in the core ($r/a < 0.5$) and wavenumber kr-spectra are measured for these discharges at the plasma edge ($r/a > 0.64$).

The spectra of a fixed-frequency reflectometer can be analyzed to study phenomena inducing electron density fluctuations. Figure 7 shows two fluctuation spectra obtained from Low-Field Side (LFS) with a Tore Supra reflectometer [29]. Both spectra are measured at $0.16 < r/a < 0.20$, one at the beginning of the density ramp-up ($n_l \sim 2.38 \times 10^{19}$ m^{-2}) and the other at the end ($n_l \sim 4.55 \times 10^{19}$ m^{-2}). At low density, specific fluctuations called Quasi Coherent (QC) oscillations can be observed around 50 kHz with the corresponding harmonic at 100 kHz. At higher density the QC disappearance suggest a modification in the turbulence nature. Recent studies indicate that TEM play a role in such fluctuations [30].

The possible dependence of intrinsic toroidal rotation profiles on a direct change in plasma parameters was investigated for several important quantities (figure 8). The normalized logarithmic density gradient $\left(R / L_{n_e} = -R \nabla n_e / n_e\right)$ at $r/a \sim 0.3$

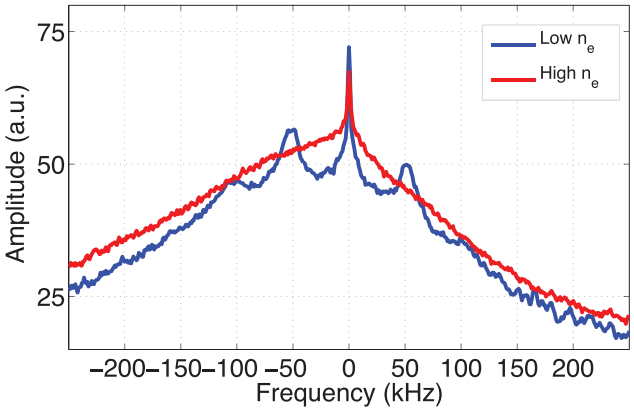

Figure 7. Turbulence spectra measured at $n_l \sim 2.38$ (—) and $\sim 4.55 \times 10^{19}$ mm^{-2} (—).

is displayed in figure 8(*a*). As suspected from the temporal evolution of the electron density profiles (figure 2(*a*)), R / L_{n_e} decreases during the density scan which means that that density profiles become flatter in the plasma core. From figures 8(*b*) and (*c*), R / L_{T_e} and R / L_{T_i} do not vary directly with density. The scatter of these quantities is due to the uncertainty in the measurements, fitting routines and spatial resolution of the diagnostics which, in turn, affects greatly the determination of the gradients. The ratio between electron and ion temperature is evaluated as a function of the line integrated density (figure 8(*d*)), and decreases as the density increases, as expected. Apart from the clear modification of the toroidal rotation in this case, no other change is noticed. Finally, the toroidal rotation gradient at mid-radius ($r/a \sim 0.4$) is depicted in figure 8(*e*)). The increase in ∇v_ϕ occurs at $n_l \sim 3 \times 10^{19}$ m^{-2}, remaining constant after $n_l \sim 3.5 \times 10^{19}$ m^{-2}.

3.3. Sawtooth activity and rotation

It is important to point out that the region where the rotation bifurcation is observed occurs inside and in the vicinity of a sawtooth inversion radius ($r/a \sim 0.25$). Therefore, the possible role of the observed sawteeth in toroidal rotation should be considered. Recent results [19] have reported that sawtooth activity may redistribute the toroidal momentum inside the

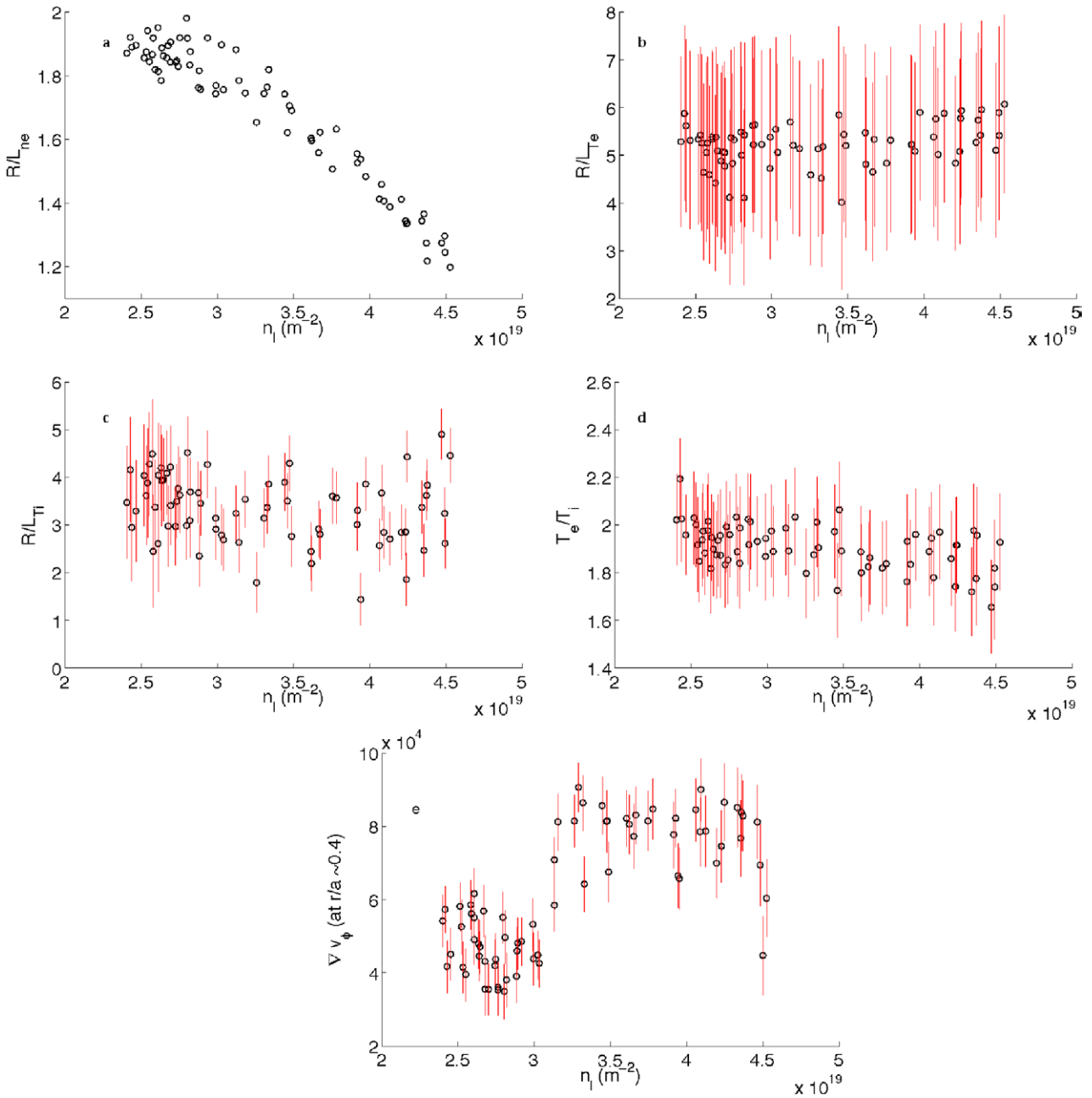

Figure 8. (*a*) R/L_{n_e}, (*b*) R/L_{T_e}, (*c*) R/L_{T_i}, (*d*) T_e/T_i as a function of line integrated density all for $r/a = 0.3$. (*e*) $\nabla\, v_\phi$ at r/a 0.4 as a function of line integrated density.

$q = 1$ rational surface, thus affecting the toroidal rotation, which could cause an increase in the co-current direction of the toroidal rotation profile inside the sawtooth inversion radius. In order to investigate the possible influence of the sawtooth activity on the experimental observations, the evolution of the sawtooth period as a function of the line integrated density has been computed (figure 9(*a*)). The grey region encompasses the density range of interest ($n_l \sim [3\text{–}3.5] \times 10^{19}$ m^{-2}), where the core toroidal rotation bifurcation is observed. The data points, represented by red dots in figure 9(*a*)), show an increase in the sawtooth period from 20 to 30 ms from the begining of the density ramp-up to $n_l \sim 3.5 \times 10^{19}$ m^{-2}, decreasing afterwards. Furthermore, the sawtooth period seems to nearly double several times during the discharge (figure 9(*a*)). Figure 9(*b*) highlights part of the discharge where an increase of the sawtooth period is appreciable. The time evolution of the ECE data countour plot is shown in figure 9(*c*), here the time interval enclosed by the black box corresponds to the increase in the sawtooth period shown by a black circle in figure 9(*a*), corresponding to a partial sawtooth crash often called a compound sawtooth. This particular type of crash has been observed during ohmic discharges reported at TFTR (see [31, 32] and references therein), where a partial reconection occurs affecting only the intermediate radii of the plasma, leaving unaffected the plasma core. The occurrence of the sawtooth crashes are marked in figure 9(*c*) with black stars, corresponding to the channel of the ECE closest to the plasma magnetic axis. Additionaly, the inversion radius is signed at

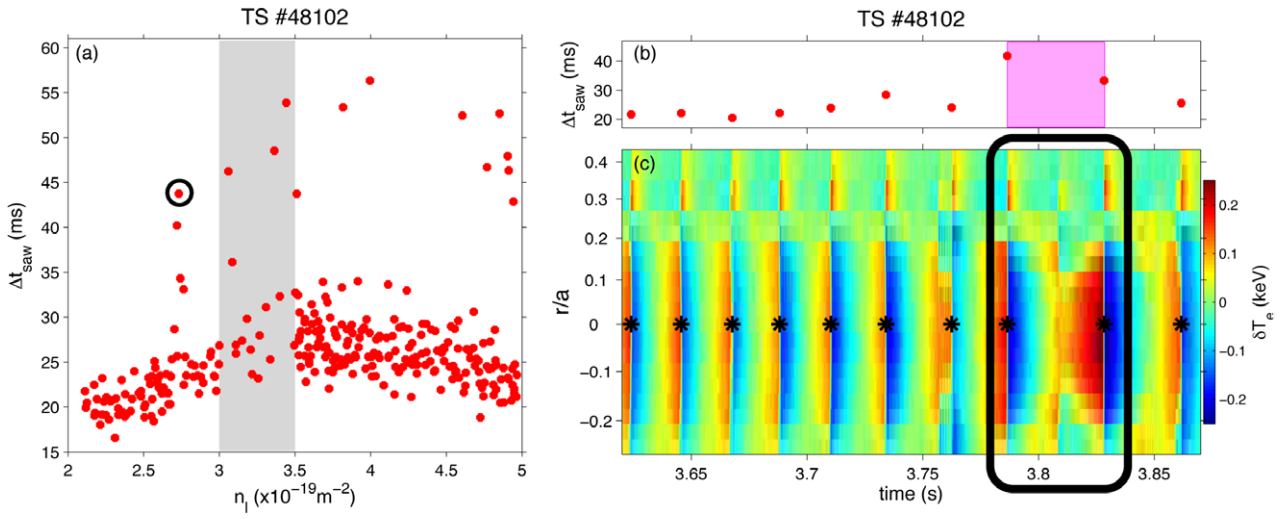

Figure 9. (*a*) Sawtooth period as a function of line integrated density. The grey region indicates the density where the core rotation bifurcation occurs in figure 4(*a*), between $n_l \sim [3\text{–}3.5] \times 10^{19}$ m^{-2}. (*b*) Part of the time evolution of the sawtooth period. The pink region highlights the instant where the sawtooth period doubles. (*c*) Part of the time evolution of the temperature for each radial position. The black box highlights the partial crash corresponding to the increase in the sawtooth period shown with a black circle star in (*a*).

$r/a \sim 0.25$. This partial crash is not detected in the inner most channels of the ECE ($r/a < 0.23$ on the LFS, figure 9(*c*)) but is visible in the mid region ($r/a > 0.27$, figure 9(*c*)). Regarding the time evolution when the partial sawtooth occurs, it is clear that this transient increase of the sawtooth period can be only atributed to the coumpound sawtooth crash. From figure 9(*a*) it can be remarked that changes in the sawtooth period occur during the entire discharge and not solely inside the region of interest. Despite the partial crashes signed inside the region of interest, we are not able to see any correlation between this data points and the observed changes in toroidal rotation seen in figure 4(*a*). If there is any relationship between these quantities, the rotation would in this case be enhanced in the counter-current direction inside the inversion radius in oposition to the described effect on TCV. Moreover, it is important to point out that no effect is appreciable outside the $q = 1$ rational surface as one should expect due to momentum conservation across the plasma profile.

In order to fully assess the influence of this sawtooth activity on plasma rotation, the Lundquist number has been computed (figure 10) to check for changes of the sawtooth dynamic during the discharge and more importantly if a significant modification occurs during the time window of interest highlighted by the grey region (between $n_l \sim 3.0 \times 10^{19}$–$3.5 \times 10^{19}$ m^{-2}). The Lundquist number is defined as $S = \tau_\eta/\tau_A$ [33], where the local resistive diffusion time is $\tau_\eta = 4\pi\bar{r}_1^2 / \eta_{||}c^2$, with $\bar{r}_1 \approx k_1^{1/2} r_1$ the average radius of the $q = 1$ surface, $k_1 = 1$ the elongation for circular Tore Supra plasmas, and the Alfvén time being defined as $\tau_A = \sqrt{3}\,R / \nu_A$. As for r_1, it is determined from the q-profile and confirmed with the inversion radius using the ECE data. The Lundquist number increases at the begining of the density ramp due to its dependence on the local resistive difusion time and decreases for the remaining of the density scan. No significant change has been observed inside the density region of interest, where the core rotation bifurcation occurs, indicating that no change in sawtooth dynamic can be linked with the change in rotation behaviour.

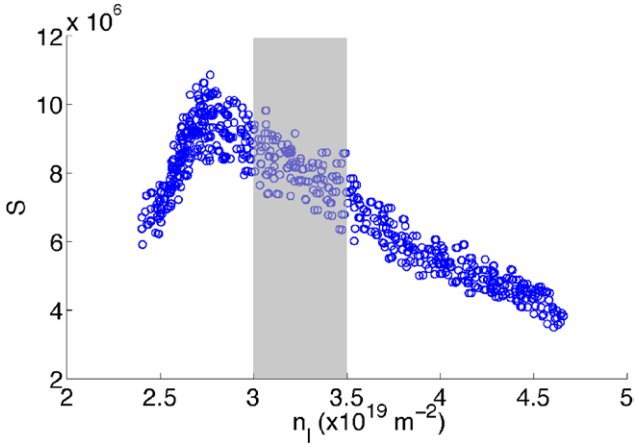

Figure 10. Lundquist number ($S = \tau_\eta/\tau_A$) plotted as a function of line integrated density. The grey region indicates the density where the core rotation bifurcation occurs in figure 4(*a*).

The evolution of the Lundquist number through the discharge can be explained by the fact that the Alfvén time increases during the discharge due to its $n_e^{1/2}$ dependency. Since the local resistive diffusion time is proportional to $T_e^{3/2}$ (and since T_e is decreasing during the discharge, as ilustrated on figure 11(*a*)), one could expect that τ_η would decrease. However, it depends also on r_1, which is found to increase significantly until $n_l \sim 3 \times 10^{19}$ m^{-2} (see figure 11(*b*)), justifing the increase of the Lunquist number at low density values ($n_l < 2.8 \times 10^{19}$ m^{-2}).

4. Comparison with neoclassical predicitions and gyrokinetic simulations

4.1. Neoclassical predictions

To gauge the experimental observations against theory, the neoclassical predictions, including the ripple-induced toroidal friction [20], is compared against the experimental

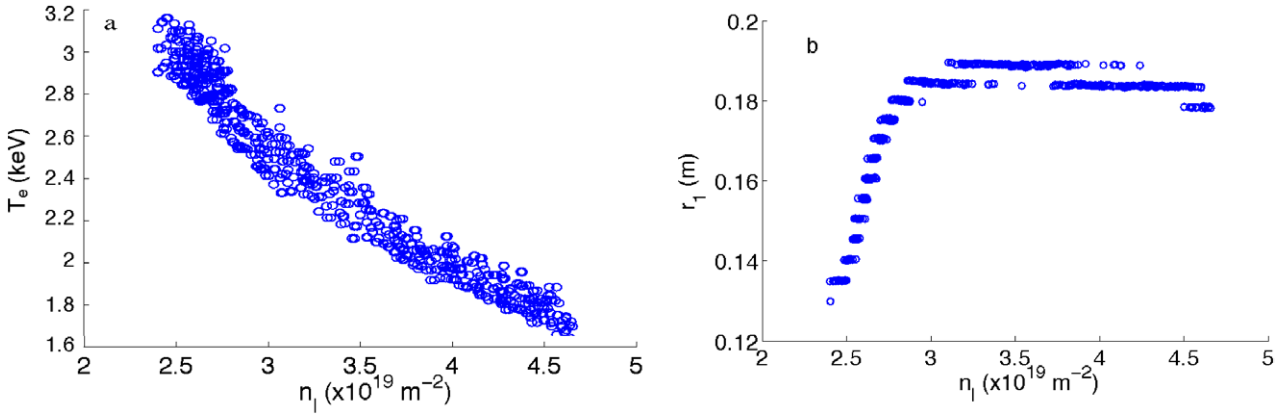

Figure 11. (*a*) Electron temperature (T_e) and (*b*) average radius of $q = 1$ surface (r_1) as function of line integrated density.

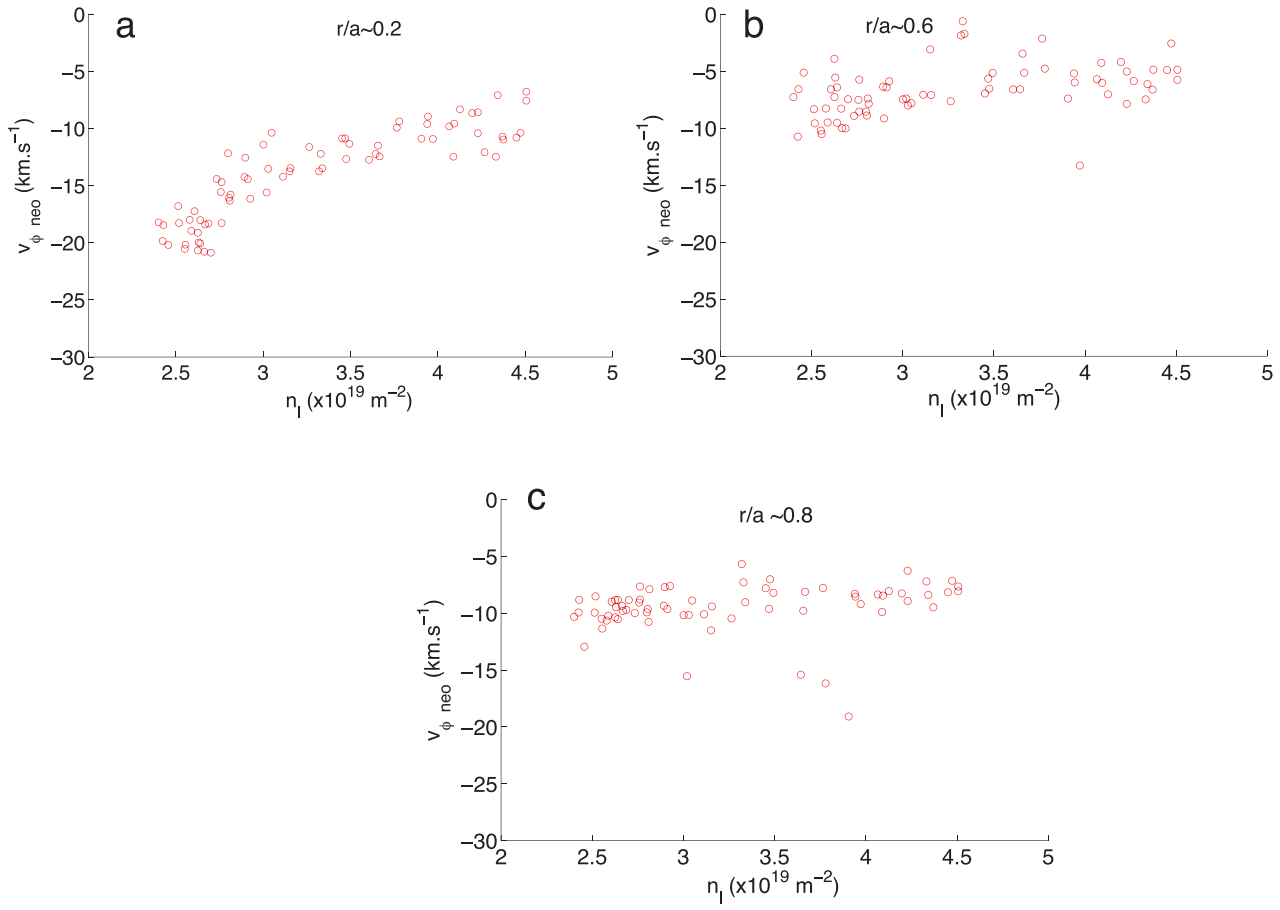

Figure 12. Toroidal velocity from collisional ripple-plateau neoclasical predictions at (*a*) *r/a* ~ 0.2, (*b*) 0.6 and (*c*) 0.8 as a function of line integrated density.

data. According to neoclassical theory, the toroidal velocity can be written as $v_\phi = k_T \nabla T_i / eZ_i B_\theta$, with $k_T = [1.67 - 3.54]$. The value of k_T is determined by the ripple amplitude and the plasma collisionality. Depending on these parameters two main regimes: banana drift and ripple plateau, are in competition. In either case, depending on the local value of collisionality, several sub-regimes can co-exist. Calculations have shown that the discharges are in ripple-plateau regime and collisional sub-regime (see [20] for further details) meaning that, in this case, $k_T = 1.67$. Here it is important to point out that the neoclassical predictions correspond to asymptotic cases and, as such, should be handled with care when directly compared with experimental results. Nevertheless, such comparison provide useful information when carried out mainly for high ripple discharges, where the competition between turbulence driven contributions and ripple induced toroidal friction is dominated by the latter. The neoclassical predictions for the deuterium toroidal velocity, $v_\phi = 1.67 \nabla T_i / eZ_i B_\theta$, are reported as a function of the line integrated density in figure 12 for a single discharge covering the whole density

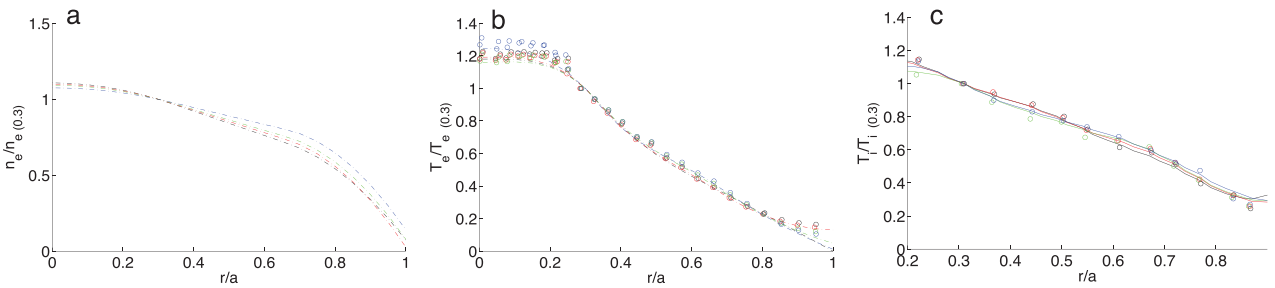

Figure 13. Normalized profiles performed at $r/a = 0.3$ of (*a*) electron density (*b*) electron and (*c*) ion temperature for four time slices.

ramp-up (see red diamond data figure 4, for $r/a \sim 0.2$, 0.6 and 0.8).

When compared to the experimentally measured values of toroidal rotation, the neoclassical predictions agree remarkably well with the experimental measurements (figure 4) in terms of magnitude and sign, but the behaviour with density differs in the core (where no bifurcation is observed) and in the intermediate region. The scatter observed for $r/a \sim 0.6$ and 0.8 can be explained by the error bars associated to ∇T_i, which is required for the neoclassical calculations, which are nonetheless consistent with experimental results discussed in section 3.1. Despite the good overall agreement, the modification of the core rotation is not reproduced by the neoclassical predictions. This indicates that this deviation is probably due to a change in the turbulence driven contributions.

4.2. Gyrokinetic analysis

The link between rotation behaviour in the plasma core and the LOC-SOC transition associated to a change of turbulence has been already established [12, 16]. In order to have a better understanding of the core toroidal rotation behaviour, turbulent stability analysis has been performed using quasi-linear gyrokinetic simulations by the QuaLiKiz code [34]. QuaLiKiz simulations were achieved using experimental profiles for the density, while the ion and electron temperature gradients were kept constant (i.e. homothetic profiles) throughout the discharge, in agreement with the experimental observations. Indeed, in figure 13 the electron density, electron and ion temperature profiles, normalized to their values at $r/a = 0.3$, show that during the density scan the shape of the density profile evolves, whereas the electron and ion temperatures are homothetic.

The gyrokinetic analysis is perfomed in the radial region where the rotation is seen to be modified, at $r/a = 0.3$, as well as for intermediate ($r/a = 0.55$) and edge plasma region ($r/a = 0.8$). In figures 14(*a*), (*c*) and (*e*), the maximum growth rate on the spectral range $k_\theta \rho_s = 0.1$–2 is plotted with its corresponding $k_\theta \rho_s$ value, whereas in figures 14(*b*), (*d*) and (*f*), the growth rates at 4 $k_\theta \rho_s$ values (0.4, 0.55, 1, 1.2) are plotted as functions of the line integrated density. As illustrated in figure 14(*a*), the plasma at $r/a = 0.3$ is found to be dominated by intermediate-scale turbulence with peak growth rate at $k_\theta \rho_s \sim 1$, indicating that trapped electron are contributing to the instabilities, which are nonetheless drifting in the ion drift direction. As the density is increased, the contribution of the high k modes is completely stabilized (figure 14(*b*)) around $n_l \sim 3 \times 10^{19}$ m^{-2}, while lower k ITG instability remains. The transition from ITG/TEM to pure ITG dominant instability when the density and, therefore, collisionality increase, may provide an explanation for the first bifurcation occuring at $n_l \sim 3 \times 10^{19}$ m^{-2} (figure 4(*a*)). Since the effect on toroidal rotation is visible from $r/a = 0$ to ~0.5, it is important to verify if the predominance of the instabilities is changing radially. The analysis of turbulent mode at mid region ($r/a = 0.55$), depicted in figures 14(*c*) and (*d*), indicates that, although trapped electrons are still contributing to the instabilities, the predominance is shifted toward lower k. As for the inner core case, the contribution of the high k modes is completely stabilized around $n_l \sim 3 \times 10^{19}$ m^{-2}, while lower k instability remains. At $r/a = 0.8$, QuaLiKiz simulations indicate that the plasma is dominated by turbulence with peak growth rate around $k_\theta \rho_s \sim 0.5$ (figure 14(*f*)), the contribution of the high k modes being far less important that in the core, here lower k ITG instability are dominant at all densities (figure 14(*e*)). Therefore the acceleration seen only in the plasma core, around $r/a = 0.3$, could be linked to a change in the nature of turbulence.

For the second rotation bifurcation occuring at $n_l \sim 3.5 \times 10^{19}$ m^{-2}, one possible mechanism could be linked to an increase in ∇v_ϕ, hence of the $E \times B$ shear, as it can be drawn from the analysis of figures 4(*a*) and (*b*) and summarized in figure 8(*e*). Indeed, sheared $E \times B$ flow is well known to contribute to the residual stress [35] and thus to the turbulent Reynolds stress. As reported in [12] both $E \times B$ and profile shearing mechanisms could be at play.

In contrast to TCV [15] and C-mod [13] observations, the measured rotation is always in the counter-current direction, likely dominated by the ripple-induced toroidal friction [18]. The latter competes with turbulent momentum which could play an important role on these observations. This will be further investigated and adressed in a future work.

5. Summary and conclusions

This paper reports on the density impact on toroidal rotation studied during density ramps in Tore Supra Ohmic plasmas combined with stationary density experiments. As observed in TCV, C-mod or Asdex-Upgrade the density can have a significant impact on plasma rotation in Tore Supra, yielding to plasma rotation bifurcation. The experimental results for toroidal rotation modification differ from the ones presented from TCV, C-mod or Asdex-Upgrade. In Tore Supra, at all

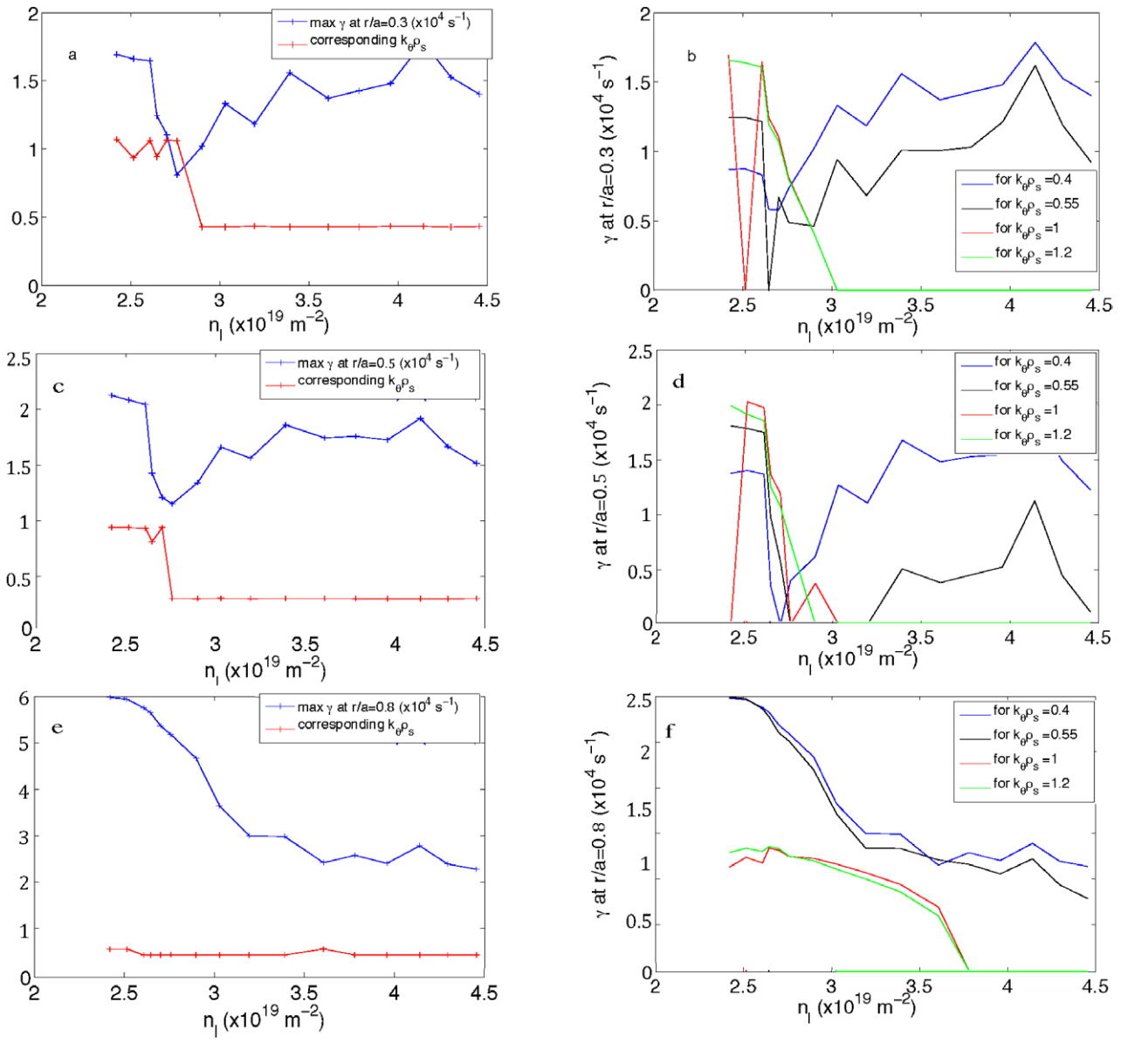

Figure 14. The maximum growth rate (blue) and respective $k_\theta\rho_s$ (red) at $r/a = 0.3$ (*a*), 0.55 (*c*) and 0.8 (*e*) and growth rate for ITG/TEM normalized wavenumber range ($0.4 < k_\theta\rho_s < 1.2$), $r/a = 0.3$ (*b*), 0.55 (*d*) and 0.8 (*f*) as a function of line integrated density.

radii the rotation is in the counter-current direction and, in the outer plasma ($r/a > 0.5$), is reduced when density increases. In the plasma core ($r/a < 0.5$), a bifurcation in rotation is seen at $n_l \sim 3 \times 10^{19}$ m^{-2}, where the the plasma accelerates, to break again at $n_l \sim 3.5 \times 10^{19}$ m^{-2}. Experimental results showing toroidal rotation breaking at all radii are in agreement with neoclassical predictions including ripple-induced toroidal friction. Nonetheless, the modification of the core rotation is not reproduced by neoclassical predictions, hence suggesting that other mechanisms are at play. The core rotation behaviour does not appear to be correlated to sawtooth activity, which leaves turbulence driven momentum flux as a possible candidate to explain the deviation from neoclassical predictions. Quasi-linear gyrokinetic simulations by the QuaLiKiz code show that in the core, the nature of linear microinstabilities changes from ITG-TEM to pure ITG at $n_l \sim 3 \times 10^{19}$ m^{-2}. Although at Tore Supra the high ripple makes the neoclassical toroidal viscosity the dominant player in setting the toroidal rotation profile, turbulent momentum transport may still be contributing. The changes that arise from the stabilization of the TEM can justify the change in rotation, most likely through a modification in the residual stress contribution, which could explain the bifurcation of the core rotation around this density.

Acknowledgments

The authors wish to acknowledge M F F Nave for the helpful discussions and useful comments to this paper.

This project has received funding from the European Union's Horizon 2020 research and innovation programme under grant agreement number 633053. IST activities also received financial support from 'Fundação para Ciência e

Tecnologia' through project Pest-OE/SADG/LA0010/2013. The views and opinions expressed herein do not necessarily reflect those of the European Commission.

References

[1] Reimerdes H *et al* 2006 *Phys. Plasmas* **13** 056107
[2] Buttery R J *et al* 2008 *Phys. Plasmas* **15** 056115
[3] Peeters A G *et al* 2011 *Nucl. Fusion* **51** 094027
[4] Eriksson L-G *et al* 2001 *Nucl. Fusion* **41** 91
[5] Eriksson L-G *et al* 2002 *Nucl. Fusion* **42** 959
[6] Eriksson L-G *et al* 2004 *Phys. Rev. Lett.* **92** 235001
[7] Eriksson L-G *et al* 2009 *Plasma Phys. Control. Fusion* **51** 044008
[8] Perkins W *et al* 2001 *Phys. Plasmas* **8** 2181
[9] Noterdaeme J-M *et al* 2003 *Nucl. Fusion* **43** 274
[10] de Vries P C *et al* 2008 *Nucl. Fusion* **48** 035007
[11] Piron L *et al* 2013 *Nucl. Fusion* **53** 113022
[12] Angioni C *et al* 2011 *Phys. Rev. Lett.* **107** 215003
[13] Rice J E *et al* 2011 *Nuc. Fusion* **51** 083005
[14] Duval B P 2008 *Phys. Plasmas* **15** 056113
[15] Bortolon A *et al* 2006 *Phys. Rev. Lett.* **97** 235003
[16] Rice J E *et al* 2012 *Phys. Plasmas* **19** 056106
[17] White A E *et al* 2013 *Phys. Plasmas* **20** 056106
[18] Fenzi C *et al* 2011 *Nucl. Fusion* **51** 103038
[19] Duval B P *et al* 2010 Momentum transport in TCV across sawteeth events *Proc. 23rd IAEA Fusion Energy Conf.* (*Daejeon, Korea, 11–16 October 2010*) paper EXS/P4-01
[20] Garbet X *et al* 2010 *Phys. Plasmas* **17** 072505
[21] Gil C *et al* 2009 *Fusion Sci. Technol.* **56** 1219
[22] Simonin A *et al* 2002 *Rev. Sci. Instrum.* **73** 2886
[23] Goldston R J 1984 *Plasma Phys. Control. Fusion* **26** 87
[24] Yushmanov P N *et al* 1990 *Nucl. Fusion* **30** 1999
[25] Hennequin P *et al* 2010 The effect of SOL flows on edge and core radial electric field and rotation in Tore Supra *Proc. 37th EPS Conf. on Plasma Physics and Controlled Fusion* (*Ireland, Dublin, 21–25 June 2010*) vol 34A p1.1040
[26] Gunn J P *et al* 2007 *J. Nucl. Mater.* **363–5** 484
[27] Clairet F *et al* 2010 *Rev. Sci. Instrum.* **81** 10D903
[28] Vermare L *et al* 2006 *Nucl. Fusion* **46** S743
[29] Sabot R *et al* 2006 *Nucl. Fusion* **46** S685
[30] Arnichand H *et al* 2014 *Nucl. Fusion* **54** 123017
[31] Yamada H *et al* 1985 *Princeton Plasma Physics Laboratory Report* PPPL-2213
[32] Nagayama Y *et al* 1996 *Nucl. Fusion* **36** 521
[33] Porcelli F *et al* 1996 *Plasma Phys. Control. Fusion* **38** 2163
[34] Bourdelle C *et al* 2007 *Phys. Plasmas* **14** 112501
[35] Gurcan O D *et al* 2007 *Phys. Plasmas* **14** 042306